nature synthesis

ARTICLES

https://doi.org/10.1038/s44160-022-00130-4

Coherent approach to two-dimensional heterolayered oxychalcogenides using molten hydroxides

Xiuquan Zhou[1], Christos D. Malliakas[2], Andrey A. Yakovenko[3], Brandon Wilfong[4], Suyin G. Wang[5], Yu-Sheng Chen[5], Lei Yu[6], Jianguo Wen[6], Mahalingam Balasubramanian[3], Hsien-Hau Wang[1], Duck Young Chung[1] and Mercouri G. Kanatzidis[1,2] ✉

Heterolayered structures consist of two or more different types of layer and can exhibit exceptional physical properties. Rational routes to synthesize new members of such compounds are required because most of these compounds have been discovered unintentionally. So far there is no generic method to vertically stack chemically different layers to form two-dimensional compounds owing to a lack of understanding of the synthesis of these materials. Here we report the use of molten hydroxides as unconventional solutions for the rapid stacking of oxide and chalcogenide layers with precise composition control. In addition, the crystal growth of heterolayered phases can be achieved by the reaction of different components at their diffusion front in molten hydroxides. This approach creates conditions in which the building blocks for each heterolayer can coexist, enabling heterolayered structures and bypassing the challenges of traditional solid-state chemistry methods where short reactant diffusion lengths predominate. This crystal growth methodology for heterolayers is also applicable to systems that do not form congruent melts at high temperatures.

Heterolayered structures, consisting of two or more chemically distinct layers stacked in sequence, usually with different anions[1], are of broad scientific interest because they can exhibit a variety of hybrid properties not encountered in the corresponding homolayered materials. Examples include the semiconductors [LnO][CuQ] (Ln = lanthanide; Q = S, Se and Te)[2,3], the cuprate $CaBa[Tl_2O_2][CuO_2]_3$ (ref. [4]) and the Fe-based superconductors $[LnO_{1-x}F_x][FeAs]$ (refs. [5,6]). The remarkable properties of these materials are derived from the possibility of fine-tuning the heterolayers. For example, the superconducting transition temperature (T_c) of $[LaO_{1-x}F_x][FeAs]$ ($x = 0.05$–0.12) is 26 K, but neither FeAs nor [LaO][FeAs] are superconductors[5]. Similarly, FeSe, a homolayered material, superconducts below 8 K (ref. [7]), but on forming $[Li_{1-x}Fe_xOH][FeSe]$, the magnetic superconductor emerges and T_c increases to 43 K (refs. [8–11]). These examples highlight the unique scientific opportunities afforded by heterolayered compounds.

One of the most outstanding challenges in stabilizing heterolayered compounds is posed by thermodynamics, because compounds with multiple components cannot easily be formed by directly heating mixtures of precursors; instead they undergo phase separation to simpler and more stable phases. The more types of element involved, the greater the probability of phase separation and incongruent melting. Johnson and co-workers used layer-by-layer vapour deposition to fabricate a variety of heterolayered chalcogenides, such as $[SnSe]_m[TiSe_2]$ (refs. [12–14]); however, oxide-containing layers were not explored because the use of oxygen in the vapour could cause the oxidation of the chalcogenide layers. The challenge to find a rational synthetic path to heterolayered compounds, such as oxychalcogenides, is to stabilize both the oxide- and chalcogenide-containing building blocks at the same time so that they can combine to assemble the correct structure. Because of the very different chemistry of the two blocks, it often happens that in most synthesis conditions one is greatly stabilized whereas the other is not, thereby giving rise to undesired phases. Therefore, the reaction medium must be sufficiently tunable in terms of reactant solubility to allow a set of conditions in which both of the building blocks are present.

Alkali hydroxide fluxes have been successfully used to grow a variety of oxide crystals, proving effective solvents for the synthesis of oxides[15,16]. When hydroxides are mixed with water in a semi-closed system, they become a new type of flux, coined as hydroflux, pioneered by zur Loye et al.[17–19]. Hydroflux is a unique reaction medium linking hydrothermal and molten bases, and it enables the discovery of new oxides and hydroxides. Hydroxides in hydroflux or as molten fluxes clearly stabilize soluble oxide building blocks during reactions. We thus hypothesized that if chalcophilic elements (also known as soft Lewis acids) were present in these fluxes, they would react more easily with soft Lewis bases, such as chalcogenides or related anions. In contrast, harder Lewis acids would prefer a harder Lewis base (oxide). This is similar to the acid–base chemistry in hydroxide fluxes explained by Lux et al.[20] as well as by Flood and Förland[21]. Therefore, a reaction environment could be created in which both soluble oxide and chalcogenide blocks could coexist. In addition, the ability to control flux basicity through the choice of alkali metal ion and the molar ratio of AOH and AX (A = alkali metal; X = halide) provides a great deal of control over the solubility of reactants and allows us to find and rationally select the correct synthesis path to the heterolayered class of

---

[1] Materials Science Division, Argonne National Laboratory, Lemont, IL, USA. [2] Department of Chemistry, Northwestern University, Evanston, IL, USA. [3] X-ray Science Division, Advanced Photon Source, Argonne National Laboratory, Argonne, IL, USA. [4] United States Naval Academy, Annapolis, MD, USA. [5] NSF's ChemMatCARS, The University of Chicago, Lemont, IL, USA. [6] Center for Nanoscale Materials, Argonne National Laboratory, Lemont, IL, USA.
✉e-mail: m-kanatzidis@northwestern.edu

compounds as well as to create many new class members in a very general way. Hence, we can rationally target heterolayers by controlling the solubility.

Although we cannot find any report on the use of neat hydroxide fluxes for chalcogenides or oxychalcogenides, interestingly, there is a hint in an alchemy recipe found in Schwartzbach, Germany in 1403 for the synthesis of philosopher's stone (HgS) involving soda ash (possibly a mixture of NaOH and Na_2CO_3)[22]. According to the phase diagram of Na_2S–NaOH, the two components are completely miscible and at 400 °C a saturated solution consists of 10 mol% Na_2S (~22–100 g NaOH)[23]. For comparison, the solubility of Li_2S in mixed LiCl–KCl (58:42), a common type of salt flux, is only 0.03% at 542 °C (ref. [24]). Therefore, chalcogenides or oxychalcogenides could be formed by controlling the ratio of A_2Q and AOH. Although AOH have been used as mineralizers for the crystal growth of metal sulfides under hydrothermal conditions, their primary function is to modulate the pH of the solution instead of serving as solvents[25,26]. When molten AOH are used as fluxes, they become solvents and reaction media, which leads to a different type of solution chemistry compared with hydrothermal reactions using AOH mineralizers. In addition, molten AOH allow the in situ formation of A_2Q through the disproportionation of chalcogens (by $6AOH + 3Q \rightarrow 2A_2Q + A_2QO_3 + 3H_2O$), obviating a separate synthesis of A_2Q. Similar disproportionation reactions have also been seen in the synthesis of chalcogenides in hydroflux[27]. Furthermore, based on the affinity of a given metal for a chalcogenide (the softer the metal ion, the stronger the affinity), we can control the oxychalcogenide assembly through acid–base chemistry. Based on this rationalization, we propose a powerful and adaptive strategy using mixed AOH and AX fluxes that enable rapid crystal growth using simple precursors of common metal halides and oxides as well as elemental chalcogens (S, Se and Te) without the need to tune their ratios. The key aspects of our method are firstly, a tunable flux by mixing hydroxides (to control basicity) and halides (to control solubility) instead of using hydroxides alone. Secondly, the demonstration of efficacy in anion systems other than oxygen, such as chalcogenides (and even pnictides). Thirdly, the tunable solubility of reactants and intermediates avoids known 'trivial' phases, which makes it a very effective strategy for the synthesis of complex multinary systems such as heterolayered mixed-anion structures. Finally, this method allows the rapid discovery of materials because the main outcome-determining synthetic parameters are temperature and flux ratio.

Here we demonstrate a general approach for the crystal growth of a large series of heterolayered $[AE_xM_yO_z][M'_2Q_2]$ (AE = Sr or Ba; M = Mn, Fe, Co, Ni, Cu or Zn; M′ = Cu, Ag or Li) and $[LaO][M'_2Q_2]$ materials[28–31]. Among these, $[Sr_2M_{1-x}O_2][(Cu_{1-y}Li_y)_2Q_2]$ (M = Mn or Ni), $[Sr_2M_{1-x}O_2][(Cu_{1-y}Li_y)_{2n}S_{n+1}]$ ($n = 2$–4), $[Sr_2Cu_{0.7}O_2][Cu_2Se_2]$, $[Ba_2Co_{0.54}O_2][Cu_2Se_2]$, $[AE_2M_{1-x}O_2][(Ag_{1-y}Li_y)_2Se_2]$ and $[Ba_3Fe_2O_5][Ag_2Se_2]$ are new compounds. In addition, we obtained an example of a heterolayer with rocksalt ($[CoSeO_2]^{4-}$) and anti-PbO ($[Cu_2Se_2]^{2-}$) layers in $Li_6[CoSeO_2][Cu_2Se_2]$. The synthesis results are described in detail in the Methods section. This work advances the synthesis science of heterolayered materials and enriches the synthetic apparatus for the more successful design of targeted compositions.

Table 1 | Synthetic conditions for oxychalcogenides in the flux of LiOH–LiCl

Reactants + Cu_2O			**Product**	**Literature**
AE/Ln	**M**	**Q**		
SrO	$MnCO_3$	S/Se	$[Sr_2Mn_{1-x}O_2][Cu_{2-y}Li_yQ_2]$	This work
SrO	$CoCO_3$	S/Se	$[Sr_2CoO_2][Cu_2Q_2]$	31,47
SrO	NiO	Se	$[Sr_2NiO_2][Cu_2Se_2]$*	This work
SrO	NiO	S	No reaction	32,33
SrO	NiO	Se + S	$[Sr_2NiO_2][Cu_2Se_{2-x}S_x]$	This work
SrO	CuO	S/Se	No reaction*	40
SrO	ZnO	S/Se	No reaction	28
BaO	$CoCO_3$	Se	$[Ba_2CoO_2][Cu_2Se_2]$	This work
La_2O_3	–	S/Se/Te	[LaO][CuQ]	48,49
Reactants + Ag_2O				
SrO	$MnCO_3$	Se	$[Sr_2Mn_{1-x}O_2][Ag_{2-y}Li_ySe_2]$	This work
La_2O_3	–	Se/Te	[LaO][AgQ]	ICDD numbers: 00-050-1794 and 04-018-8540

The symbol * represents oxidized Ni or Cu species, which will be discussed later. The International Centre for Diffraction Data (ICDD) includes the diffraction data of LaOAgSe (00-050-1794) and LaOAgTe (04-018-8540).

Results and discussion

Reaction chemistry to two-dimensional oxychalcogenides. In a typical reaction to form oxychalcogenides, a source of alkali earth metal, AEO or $AE(OH)_2$, a source of transition metal, MCO_3, MO or MCl_2, Cu_2O and elemental chalcogen were mixed with LiOH–LiCl. We could tune the basicity of the flux by means of the LiOH/LiCl ratio and the compositional ratio of LiOH, defined as mol LiOH/(mol LiOH + mol LiCl), between 0.5–1, where 0.65 gave a eutectic melt at 285 °C. Here, molten LiOH was the solvent and LiCl served to tune the basicity further. The reactants were typically used in a stoichiometric ratio, and the molar ratio between reactants and flux was typically around 1:10 to ensure good dissolution. In these reactions, hydroxide supplied the extra O^{2-}. As the reactions were carried out above 500 °C, the excess water formed during the reaction probably evaporated. After the disproportionation of the chalcogen and dissolution of all the precursors at 500 or 600 °C, a generic equation for the ionic reaction can be described as follows:

$$2AE^{2+} + M^{2+} + 2Cu^{+} + O^{2-} + 2Q^{2-} + 2OH^{-} \rightarrow [AE_2MO_2]\,[Cu_2Q_2] + H_2O \qquad (1)$$

For comparison, the following equation describes the solid-state synthesis of similar oxychalcogenides by mixing SrS, M and CuO in a sealed silica tube at 920 °C for 24 h (ref. [28]):

$$2SrS + M + 2CuO \rightarrow [Sr_2MO_2]\,[Cu_2S_2] \qquad (2)$$

We summarize the reactions and products in Table 1. We found that different chalcogen sources, such as S, Li_2S or SrS, did not affect the final product, which suggests that the disproportionation reaction of elemental Q to form in situ Q^{2-} is very effective. Therefore, unlike in solid-state reactions, the extra step to prepare alkali earth chalcogenide precursors, such as SrS, is not needed[28]. We carried out reactions for M = Mn, Co, Ni, Cu and Zn for both Q = S and Se and obtained 0.08–0.1 mm crystals of $[Sr_2Mn_{1-x}O_2][Cu_{2-y}Li_yQ_2]$ (Supplementary Tables 1 and 2 and Supplementary Fig. 1), $[Sr_2CoO_2][Cu_2Q_2]$ (Supplementary Tables 3 and 4) and $[Sr_2NiO_2][Cu_2Se_2]$ (Supplementary Table 5). The crystals obtained at 600 °C were generally larger than those prepared at 500 °C, but the sizes of the crystals did not show significant differences for cooling rates of 4, 7 or 10 °C h^{-1} and the faster cooling of furnace switch-off. For M = Ni and Q = S, only Ni_3S_2 and Cu or Cu_2S were recovered, although $[Sr_2CoO_2][Cu_2S_2]$ has been reported[32,33]. We attribute this to the high sulfur affinity of Ni. For M = Cu, the as-recovered product was digenite ($Cu_{1.8}S$) or Cu_2Se without any CuO, indicative of the reduction of Cu^{2+} by the S^{2-} ions in the hydroxide flux.

Table 2 | Synthetic conditions for heterolayered oxychalcogenides in the flux of NaOH–NaI

Reactants + Cu_2O			Product	Literature
AE	M	Q		
SrO	$MnCl_2$	S/Se	$[Sr_2Mn_{1-x}O_2][Cu_2Q_2]$	28
BaO	$MnCl_2$	Se	$[Ba_2Mn_{1-x}O_2][Cu_2Se_2]$	This work
SrO	$FeCl_2$	Se	$[Sr_3Fe_2O_5][Cu_2Se_2]$	35
Reactants + Ag_2O*				
SrO/BaO	$MnCl_2$	Se	$[AE_2Mn_{1-x}O_2][Ag_{2-y}Se_2]$	31,50
BaO	$FeCl_2$	Se	$[Ba_3Fe_2O_5][Ag_2Se_2]$	This work
SrO/BaO	$CoCO_3$	Se	$[AE_2CoO_2][Ag_2Se_2]$	50
BaO	NiO	Se	$[Ba_2NiO_2][Ag_2Se_2]$	34
BaO	CuO	Se	$[Ba_2CuO_2][Ag_2Se_2]$	34
BaO	ZnO	Se	$[Ba_2ZnO_2][Ag_2Se_2]$	51

*When LiOH was added as a reactant to substitute Ag in the $[Ag_2Se_2]^{2-}$ layer, the afforded crystals were larger and of better quality.

To assess how adaptive this synthetic method is, we explored the reaction with AE = Ba, M = Co and Q = Se targeting $[Ba_2CoO_2][Cu_2Se_2]$, which is not reported in the literature. We obtained black crystals of $[Ba_2Co_{0.54}O_2][Cu_2Se_2]$ (Supplementary Table 6). When we used Ln instead of AE, we could obtain all known compounds of the [LaO][CuQ] family[32], [LaO][AgSe] and [LaO][AgTe] (Supplementary Fig. 2). These reactions also afforded red crystals (up to 0.3 mm) of $[Sr_2Mn_{1-x}O_2][Ag_{2-y}Li_ySe_2]$ (Supplementary Table 7 and Supplementary Fig. 3). These results demonstrate the applicability of this hydroxide flux method to a variety of heterolayered oxychalcogenide systems.

On targeting the $[AE_2MO_2][Ag_2Se_2]$ family, only M = Mn was successful with the LiOH–LiCl flux; M = Co, Ni, Cu and Zn all afforded similar ternary compounds of AE-Ag-Se, not reported in literature. This suggests competing trivial phases (binaries or ternaries) are more favourable for the silver system, which can be attributed to the lower solubility of the silver selenides compared with the copper selenides. Therefore, we postulated that the crystallization would shift towards more complex heterolayers if the solubility of the ternary phases were increased to prevent their precipitation. This hypothesis was proved correct by conducting the reactions in a more basic NaOH–NaI flux, which enables higher solubility. As shown in Table 2, we were able to grow crystals of $[Ba_2MO_2][Ag_2Se_2]$ for M = Mn, Co, Ni, Cu and Zn (Supplementary Tables 8–11). This is quite remarkable because the M = Ni and Cu compounds have only previously been reported to have been prepared under high pressure (7–15 GPa) above 850 °C (ref. [34]). Because of the high solubility of ZnO and ZnSe, which are the dominant phases of the reactions in LiOH–LiCl, these trivial binary phases were not found in the NaOH–NaI flux. In another illustrative example, because of the high affinity of Fe towards chalcogenides, we were not able to obtain any intergrowth compounds in the LiOH–LiCl flux, whereas using NaOH–NaI, we grew crystals of $[Sr_3Fe_2O_5][Cu_2Se_2]$ (ref. [35]) and the new compound $[Ba_3Fe_2O_5][Ag_2Se_2]$ (Supplementary Table 8). Thus, by tuning the solubility, we can shift the direction in favour of heterolayers against trivial phases.

The aforementioned oxychalcogenides consist of separate metal oxide–chalcogenide layers, but there is another class of oxychalcogenide consisting of a metal centre that binds to O and Q simultaneously, such as CaCoOS, BaCoOS, Li_2CoOQ and CaFeOSe (refs. [36–38]). Such bonding types can be achieved with reaction temperatures below 500 °C in LiOH–LiCl, and we have successfully grown crystals of BaCoOS, Li_2CoOS and Li_2CoOSe. In addition, we have found that even slices of the three-dimensional antiperovskite type Li_2CoOSe can be used as a basic building block to form the new heterolayered $Li_6[CoSeO_2][Cu_2Se_2]$ by adjusting the solution chemistry using hydroxide fluxes. Therefore, our method provides a way to design heterolayered structures based on the lattice matching of different building blocks.

Crystal structures of $[Sr_2Mn_{1-x}O_2][Cu_{2-y}Li_yQ_2]$. We found that when M = Mn the products were quite different from the reported $[Sr_2MnO_2][Cu_{1.5}Q_2]$ compounds prepared by the standard solid-state reaction chemistry described in equation (2)[29,30]. The compound $[Sr_2MnO_2][Cu_{1.48}S_2]$ has a tetragonal space group of $I4/mmm$ ($a = 4.0139(2)$ Å and $c = 17.1663(9)$ Å)[29]. Similarly, the Se analogue has lattice constants of $a = 4.06955(7)$ Å and $c = 17.8999(3)$ Å and a composition of $[Sr_2MnO_2][Cu_{1.5}Se_2]$ (ref. [30]). Both compounds are black because of the free-carrier absorption of the metallic state created by Cu vacancies during the 920 °C synthesis. In contrast, our crystals of $[Sr_2Mn_{1-x}O_2][Cu_{2-y}Li_yQ_2]$ are transparent yellow and brown for Q = S and Se, respectively (Supplementary Fig. 1), and the lattice parameters of c, indicative of interlayer spacing, are much larger at 17.923(1) and 18.591(1) Å, respectively. The big differences in interlayer spacing and colour suggest we have different compounds and the lattice expansion can be explained by Li substitution at the Cu site. Li substitution at the Cu site was reported by Rutt et al. using post-synthetic lithiation up to complete removal of Cu (ref. [39]). Similarly, $[Sr_2Mn_{0.56}O_2][Ag_{1.84}Li_{0.16}Se_2]$ has lattice parameter $c = 19.591(4)$ Å, which is notably larger than that of $[Sr_2MnO_2][Ag_{1.5}Se_2]$ ($c = 19.1179(2)$ Å)[31].

Using high-resolution single-crystal X-ray diffraction (SXRD) at the Advanced Photon Source, we discovered that these Mn oxychalcogenides are in fact a series of $[Sr_2Mn_{1-x}O_2][(Cu_{1-y}Li_y)_2Q_2]$ with a $\sqrt{2} \times \sqrt{2}$ superstructure in the a–b plane (Fig. 1a and Supplementary Table 1). The superstructure results from Mn vacancy ordering (Fig. 1b), where the Mn1–O_4 squares are compressed and the Mn2–O_4 squares are elongated. As a result, Mn favours the site with the stronger Mn–O bond (Mn1), and the larger the occupancy difference between the two Mn sites, the stronger the superlattice reflections (Supplementary Fig. 4). The high-resolution transmission electron microscopy (HRTEM) image in Fig. 1e clearly shows the two sites. In the Se analogue, the Mn2 site is completely vacant, whereas the Mn1 site is fully occupied. In addition, Li atoms partially replace Cu atoms, causing the interlayer spacing to expand linearly with the fraction of Li^+ (Fig. 1c).

Phase formation control with tunable basicity. Having determined the structures of the new Mn oxychalcogenides, we could establish a correlation between Li occupancy and the synthetic conditions using Vegard's law (Fig. 1d). We found that increasing the basicity or reaction temperature resulted in higher Li occupancy. These two parameters can actually be unified as a single parameter, basicity, because higher temperature increases the dissociation of LiOH thus increasing the basicity[15,16]. To test this hypothesis, we carried out a reaction in which we replaced LiCl with LiI. Because the I^- ion is larger and more polarizable than Cl^-, this effectively reduces the hardness (basicity) of the medium. The as-recovered sulfide crystals synthesized using LiOH–LiI with a compositional ratio of LiOH of 0.6 at 500 °C were a much darker colour with a smaller interlayer distance of 17.733(3) Å, about 0.15 Å smaller than similar samples prepared with LiOH–LiCl (Supplementary Fig. 5). This suggests a smaller degree of Li substitution (about 22%, extracted using Vegard's law) at the Cu site compared with in the LiCl medium.

To further understand the effect of basicity on the reaction path, we carried out reactions without any molten hydroxide (LiOH), instead using mixed LiCl–LiI at a temperature comparable to that used with the LiOH–LiCl flux. These reactions afforded only trivial binary phases, such as MnS, $Cu_{2-x}S$ or SrO, without any

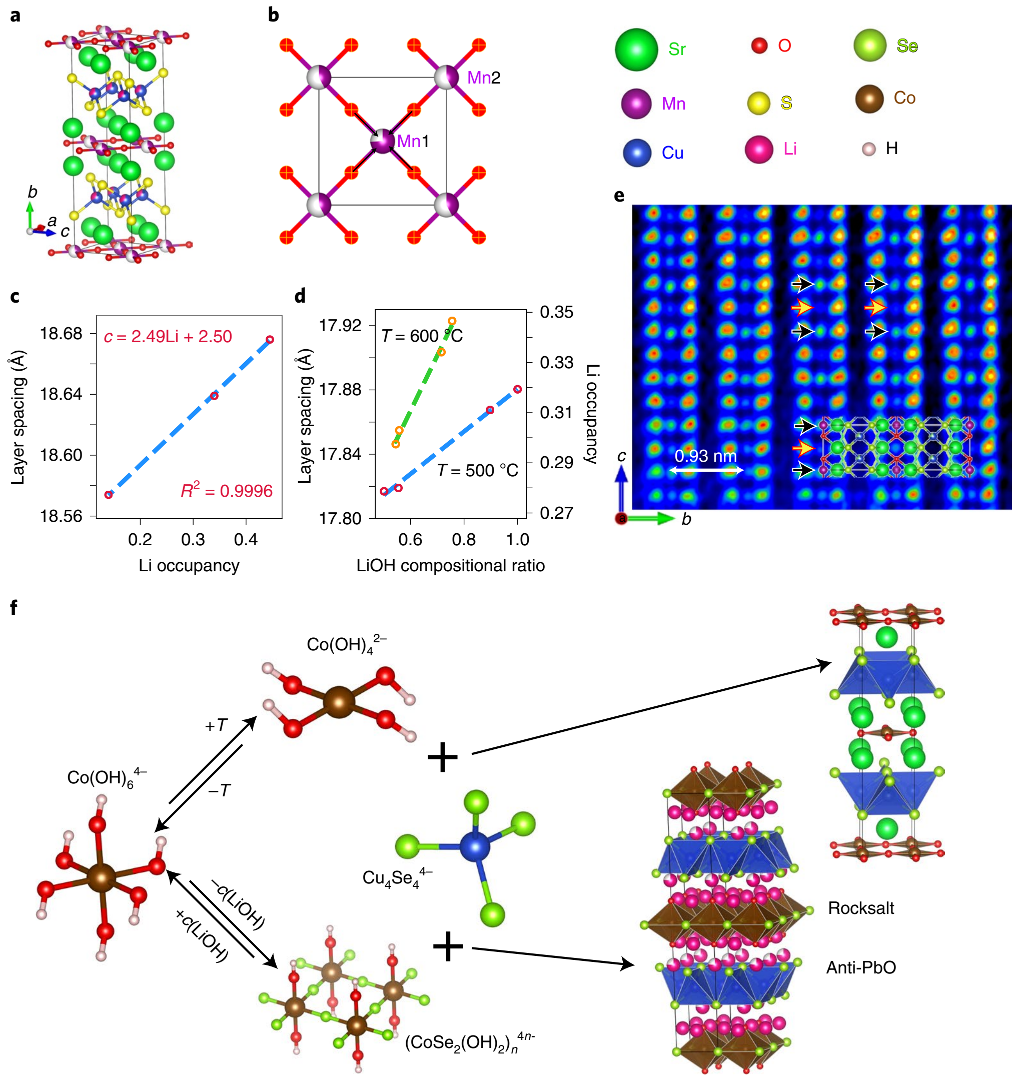

Fig. 1 | Crystal structures and formation paths for $[Sr_2Mn_{1-x}O_2][Cu_{2-y}Li_yQ_2]$ heterolayers. a,**b**, Crystal structure of $[Sr_2Mn_{0.58}O_2][Cu_{1.36}Li_{0.64}S_2]$ solved by synchrotron SXRD (**a**) and its Mn vacancy-ordered superlattice (**b**). The bond length of Mn1–O is reduced to 1.9463(7) Å and the Mn2–O elongated to 2.0157(7) Å. The atom colour code is shown in the top right of the figure and applies to all figures. **c**, Li occupancy (= $y/2$) for $[Sr_2Mn_{1-x}O_2][(Cu_{1-y}Li_y)_2Se_2]$ as a function of interlayer distance (c), as determined by SXRD. R is the coefficient of determination, indicating the goodness of fit. **d**, Interlayer distance and Li occupancy for $[Sr_2Mn_{1-x}O_2][(Cu_{1-y}Li_y)_2S_2]$ for samples synthesized by tuning the basicity at 500 and 600 °C. The interlayer spacing in **d** was determined from the PXRD data and the corresponding Li occupancy was estimated using Vegard's law, determined from the correlation extracted from SXRD. **e**, HRTEM image of the vacancy-ordered superlattice of $[Sr_2Mn_{1-x}O_2][(Cu_{1-y}Li_y)_2Se_2]$. The sites of Mn1 and Mn2 are marked by black and yellow arrows, respectively. The contrast difference between these sites is consistent with the single-crystal model suggesting higher Mn occupancy for site Mn1. **f**, Reaction scheme for the stacking of different types of layers by changing the temperature and basicity. Lower temperature (T) and LiOH concentration (c(LiOH)) favour the stacking of the octahedrally coordinated Co-containing layers in the compound $Li_6[CoSeO_2][Cu_2Se_2]$ (bottom right structure), formed from the reaction of Cu_4Se_4 with $[CoSe_2(OH)_2]_n$, instead of $[Sr_2CoO_2][Cu_2Se_2]$ (top left structure).

oxychalcogenides (Supplementary Fig. 6), highlighting the critical role of hydroxides in forming heterolayered oxychalcogenides.

This solution chemistry was also investigated for M = Co, Ni and Cu. For M = Co with a stoichiometric ratio of $CoCO_3$/SrO/Cu_2O/Q = 1:2:1:2 at 500 °C, no oxychalcogenide formed (Supplementary Figs. 7 and 8 and Supplementary Tables 3 and 4). However, when the ratio was raised to 3:2:1:2, crystals of $Sr_2CoO_2Cu_2Q_2$ without any Li substitution were obtained at 500 °C along with a minor unknown phase. Pure $Sr_2CoO_2Cu_2Q_2$ crystals were obtained at 600 °C (Supplementary Fig. 7c).

A closer look at the reactions at 500 °C revealed that the minor phase is a new type of heterolayered compound $Li_6[CoSeO_2][Cu_2Se_2]$ (Fig. 1f and Supplementary Table 12) with stacked rocksalt $[CoSeO_2]^{4-}$ and anti-PbO-type $[Cu_2Se_2]^{2-}$ layers. It is likely that an equilibrium exists between different Co complexes in the molten base solution whose concentrations can be controlled by temperature, suggesting a new avenue for controlling heterolayered compounds by tuning the metal coordination geometry.

For M = Ni, we observed the formation of Ni_3S_2 and $Cu_{2-x}S$ with the LiOH–LiCl flux (LiOH compositional ratio between 0.5 and 0.65), whereas when neat LiOH was used, Ni^{2+} was reduced to Ni metal. In comparison for Q = Se, when the concentration of either LiOH or Q^{2-} was decreased, $[Sr_2NiO_2][Cu_2Q_2]$ was obtained without any Li substitution at the Cu sites of the structure (Supplementary Table 5). For M = Cu, no $[Sr_2CuO_2][Cu_2Q_2]$ was formed with a LiOH compositional ratio as low as 0.5, leading to mixtures of CuQ,

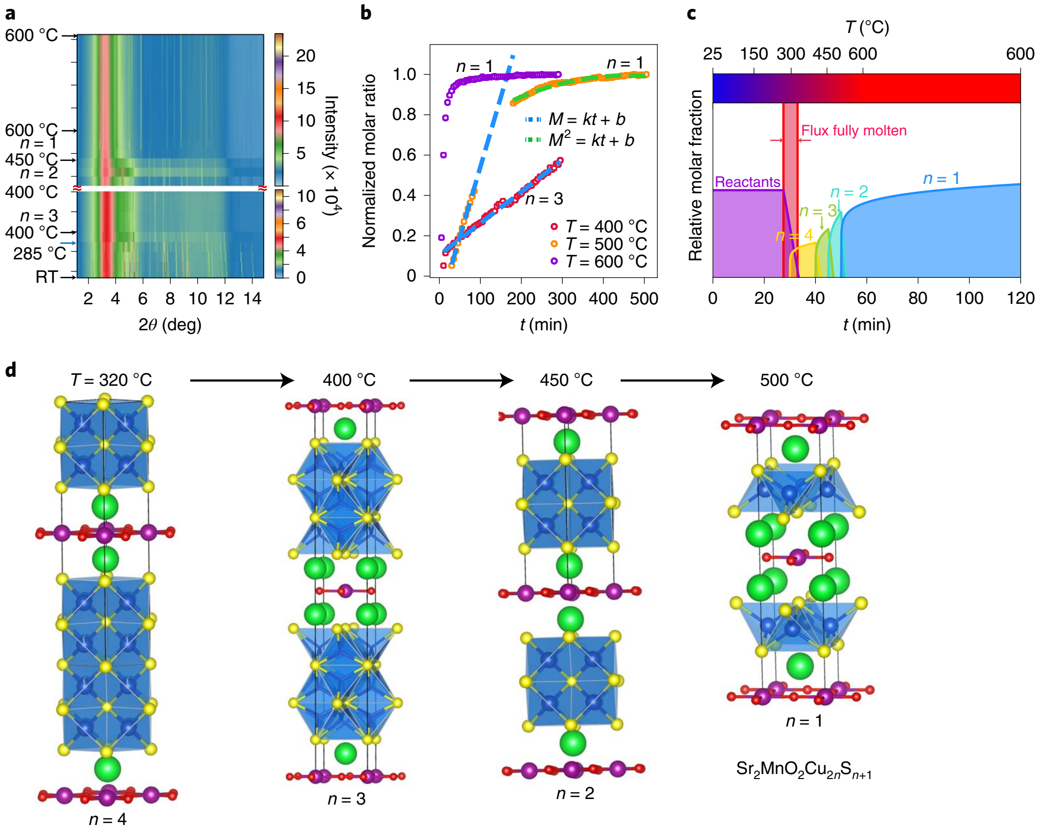

Fig. 2 | Panoramic synthesis to explore reaction pathways to $[Sr_2Mn_{1-x}O_2][(Cu_{1-y}Li_y)_2Q_2]$ in molten LiOH–LiCl. Panoramic synthesis was performed using in situ PXRD to monitor the reaction pathways leading to $[Sr_2Mn_{1-x}O_2][(Cu_{1-y}Li_y)_2Q_2]$ in molten LiOH–LiCl as a function of temperature and time. **a**, Contour plot of in situ reactions at 400 and 600 °C. The blue arrow indicates the eutectic melting point of the LiOH–LiCl flux at 285 °C. The contour plot measured at 500 °C, similar to the 600 °C reaction, is shown in Supplementary Fig. 9. The isothermal reaction stage at 400 °C has been omitted from the graph and only the heating stage from 400 to 450 °C is shown above the break in the graph. The colour gradient gives the scale of the dimensionless intensities of each one-dimensional (1D) diffraction pattern of the two-dimensional map. RT, room temperature. **b**,**c**, Kinetics at different temperatures (**b**) and the corresponding phase map (**c**). The dotted blue and green lines in **b** show the fits for zero-order and diffusion-limited reactions, respectively. *M* and *t* are normalized molar ratio and reaction time for *y*- and *x*- axes, respectively and *k* and *b* are constants for linear fit to correlate *M* with *t*. The phase map shown in **c** was constructed on the basis of the ex situ reactions and in situ studies reported in **b** and not on actual data points. **d**, Ex situ reactions reproducing $[Sr_2Mn_{1-x}O_2][(Cu_{1-y}Li_y)_{2n}S_{n+1}]$ ($n = 1$–4).

$Cu_{2-x}Q$ and Cu. We presume that Cu^{2+} can oxidize Q^{2-} in molten LiOH, which explains why no Cu^{2+} species was present after the reaction. However, this can be mitigated by separating CuO from the chalcogen source in the reaction vessel using a diffusion-driven approach. We could obtain $[Sr_2Cu_{1-x}O_2][Cu_2Se_2]$ using this kinetic method, but not by mixing all the precursors[40].

Kinetics and crystal growth by panoramic synthesis. To understand the reaction and crystal growth mechanism of the heterolayered oxychalcogenides, we monitored the full reaction paths panoramically (Fig. 2a–c) using synchrotron powder X-ray diffraction (PXRD) collected at beamline 17-BM of Advance Photon Source. In addition to the progress of reactions, this panoramic reaction analysis revealed at 400 °C a new tetragonal heterolayer phase with $a = 4.055(3)$ Å and $c = 31.62(2)$ Å as an intermediate (Supplementary Fig. 10). Conceptually, this is the $n = 3$ member of the homologous series $[Sr_2MnO_2][Cu_{2n(1-x)}S_{n+1}]$ ($n = 1$–3)[29]. The reported $n = 3$ structure exhibits a similar tetragonal lattice with $a = 4.0057(2)$ Å and $c = 28.296(2)$ Å (note these values are for room temperature).

When heating the reaction mixtures from room temperature to 600 °C, an intermediate phase briefly appeared above 450 °C (Fig. 2a) and quickly converted to the $n = 1$ phase above 500 °C. Informed by this observation, we carried out ex situ reactions at different temperatures to isolate the new phases. We successfully isolated three additional phases as black crystals at 320, 400 and 450 °C. We determined that the product at 320 °C is $[Sr_2MnO_2][Cu_{7.26}S_5]$ with a $P4/m$ space group and $a = 3.911(6)$ Å and $c = 16.79(4)$ Å (Supplementary Table 13). Interestingly, this compound, which is the $n = 4$ member of the $[Sr_2MnO_2][Cu_{2n(1-x)}S_{n+1}]$ series, does not have the Mn atom vacancies observed in the $n = 1$ phase. We further determined that the compounds prepared at 400 and 450 °C are the $n = 3$ and 2 members of the homologous series, respectively. Because of poor data quality, we were only able to index their unit cells. It is interesting to note that the $n = 2$ phase exhibits an incommensurate cell with $a = 5.610(1)$ Å and $b = 5.613(1)$ Å and an incommensurate vector of $\boldsymbol{q} = 0.234(1)\boldsymbol{a}^* + 0.235(1)\boldsymbol{b}^*$, where $\boldsymbol{a}^*$ and $\boldsymbol{b}^*$ are reciprocal lattice vectors, in the basal plane (Supplementary Fig. 11a). Elemental analysis suggested no Mn vacancies (Supplementary Fig. 11b). The precise structure will be the subject of future research.

These panoramic reaction experiments revealed that the layer thickness can be controlled by temperature and that the crystallization of the oxychalcogenides is very fast. They also informed on the precise control of the heterolayers and shone a light on how the heterolayered homologous structures form[41]. For the isothermal reactions at 500 and 600 °C, the crystallization plateaued at about 3

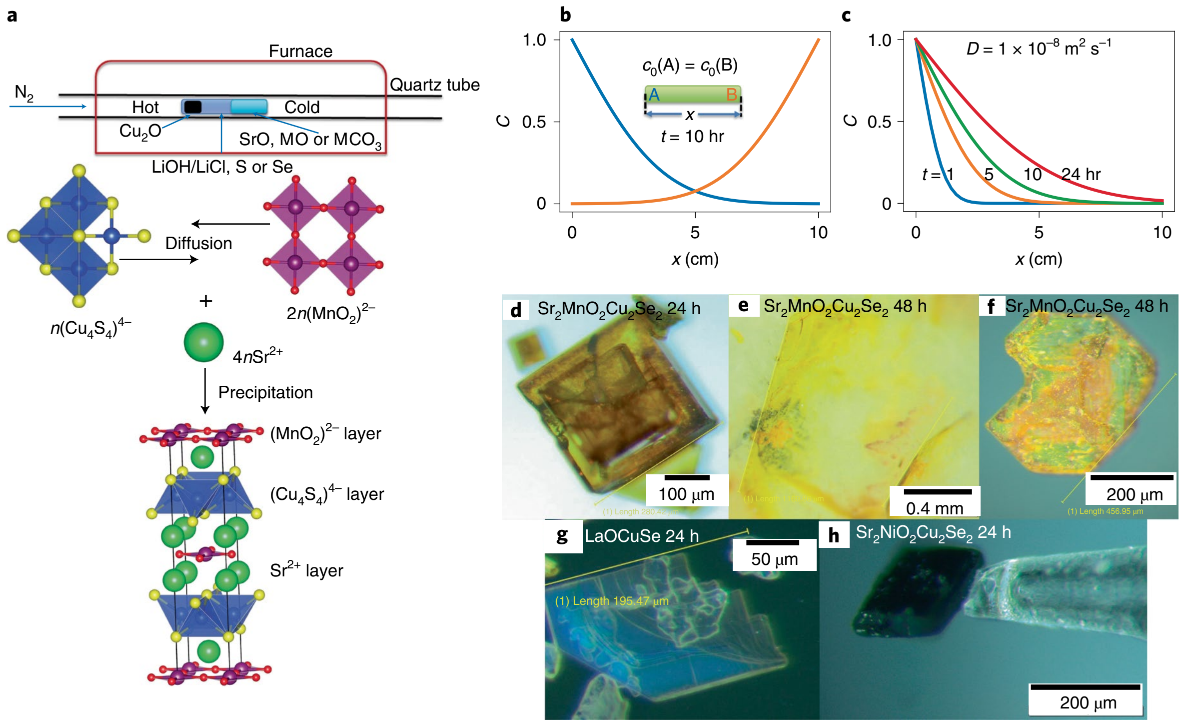

Fig. 3 | Crystal growth by diffusion. a, Reaction set-up and schematic of the vertical stacking of the heterolayers by diffusion of the respective building blocks. **b**,**c**, Ideal 1D diffusion of components A and B placed at either end of a container (**b**) and concentration distribution over time (**c**). In **b** and **c**, D is the diffusion coefficient, x represents the distance (in cm) from the left end of the container and C is the ratio of the concentration of each component to the initial concentration c_0 at distance x; in **b**, the blue line represents C for component A, and the red line represents C for component B. **d**–**h**, Optical images of the diffusion-driven crystal growth of crystals of $[Sr_2Mn_{1-x}O_2][(Cu_{1-y}Li_y)_2Se_2]$ for 24 h (**d**), a thin crystal of $[Sr_2Mn_{1-x}O_2][(Cu_{1-y}Li_y)_2Se_2]$ up to 1 mm for 48 h (**e**), a thicker crystal of $[Sr_2Mn_{1-x}O_2][(Cu_{1-y}Li_y)_2Se_2]$ up to 0.5 mm for 48 h (broken during handling) (**f**), [LaO][CuSe] for 24 h (**g**) and $[Sr_2Ni_{0.7}O_2][Cu_2Se_2]$ for 24 h (**h**).

and 1 h, respectively (Fig. 2b). This suggests that the crystal growth process is not controlled by cooling, as one may think, but during the initial precipitation reaction.

Diffusion-driven kinetic method. In traditional solid-state chemistry, crystal growth is generally pursued by cooling a congruent melt or cooling the ingredients dissolved in a flux. In both cases, all the components are thoroughly mixed to minimize the diffusion length to afford a pure homogeneous product and avoid localized impurities. Often reactants are pressed together in pellets to ensure complete reaction. Thus, growing single crystals by separating the starting materials is counterintuitive for conventional solid-state reactions. However, from the point of view of solution chemistry, this approach is supported in practice, for example, in crystal growth by diffusion, at the interface of two solvents and in gels[42–44]. We adapted these practices to the molten hydroxide fluxes by placing the oxide- and chalcogenide-forming reagents at different locations in a reaction vessel and then allowing them to diffuse across the solution in opposite directions. We observed that the heterolayers can be stabilized by co-precipitation of different components at their diffusion front at high temperature. This is possible if the following two requirements for the host solvents are met: firstly, a relatively low melting temperature to keep the precipitates kinetically stable and secondly, the ability to dissolve substantial amounts of the chemical building blocks. In contrast, when all the reagents were mixed in the same location, intermediates can form in close contact with each other and thereby combine and the target phases precipitate too quickly, forming polycrystalline powders. Therefore, separating reactants in molten hydroxides is highly effective for growing crystals of heterolayered materials.

We used Fick's law of diffusion to formulate the model shown in Fig. 3a–c with the details described in the Methods section in the Supplementary Information. Using this approach for M = Mn, crystals up to 1 mm were grown for the first time over a 48-h diffusion period, one order of magnitude larger than by direct mixing in molten bases and two to three orders of magnitude larger than in solid-state reactions (Fig. 3d–f). For shorter reaction times of 24 h, smaller crystals were obtained (up to 0.4 mm), which is consistent with our hypothesis. Semiconductors of [LaO][CuQ] are notoriously difficult to grow, and we have not found any report of the crystal growth of [LaO][CuSe]. For a 24-h diffusion period, we were able to obtain crystals larger than 0.2 mm (Fig. 3g) with high phase purity (Supplementary Fig. 12). These results show that this diffusion-driven crystal growth approach is universal and applicable to many incongruently melting compounds.

This diffusion-driven crystal growth enabled the formation of 0.3 mm crystals of $[Sr_2Ni_{0.7}O_2][Cu_2Se_2]$ (Supplementary Table 14 and Supplementary Fig. 13a) and 0.1 mm crystals of $[Sr_2Cu_{0.7}O_2][Cu_2Se_2]$ (Fig. 3h, Supplementary Table 15 and Supplementary Fig. 13b) using neat LiOH. This is surprising because Ni^{2+} and Cu^{2+} tend to be fully reduced to metallic Ni and Cu, respectively, when mixed with Se^{2-} at high LiOH concentrations. By not loading any Se at the oxide source end of the reaction vessel, only NiO or CuO, the dissolved Ni^{2+} and Cu^{2+} can diffuse to the centre of the container 'unscathed'. Then precipitation of Ni^{2+}/Cu^{2+} or even Ni^{3+}/Cu^{3+} with $[Cu_2Se_2]^{2-}$ (a Cu^+-containing block) out of solution allows them to form oxychalcogenides before being reduced to the metals. This diffusion-driven strategy using starting materials separated at the opposite ends of a reaction vessel provides a coherent approach to kinetically stabilizing heterolayers

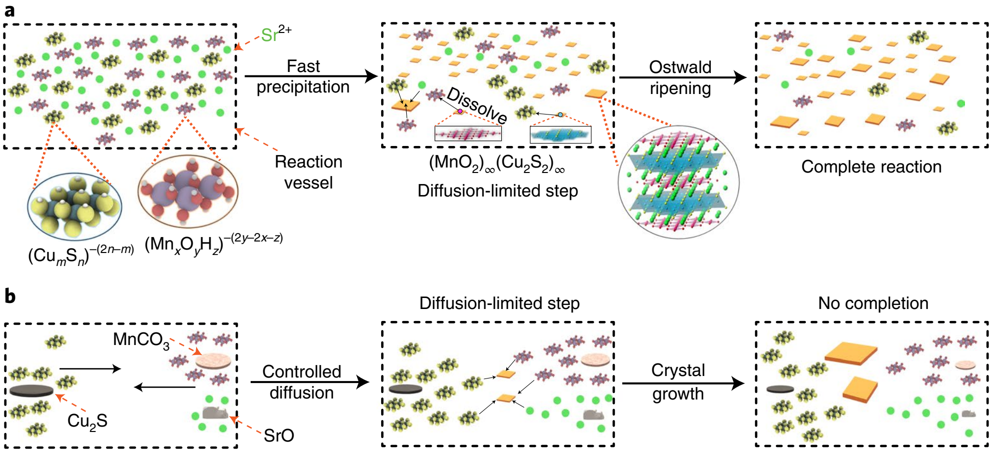

Fig. 4 | Crystal growth processes. **a**, Reaction of mixed starting materials: the binary starting materials initially dissolve (left), a large number of nuclei form by fast precipitation (middle) and micrometre-sized crystals grow from the nuclei (right). **b**, Diffusion-driven reactions with separated starting materials: dissolved binary starting materials diffuse to the centre of the reaction vessel from opposite sides (left), a small number of nuclei form at the diffusion front (middle) and these nuclei grow into larger crystals (right).

even with very oxidizing Ni^{3+}/Cu^{3+} ions in $[Sr_2M_{0.7}O_2]^{2+}$ using molten hydroxides.

Crystal growth process. Suggest a two-stage reaction sequence with a zero-order reaction at the beginning and a diffusion-limited one close to completion of the reaction. Here, we elaborate on this phenomenon from the point of view of reactions occurring in solution. As indicated in Fig. 2a, once the flux is molten, almost all the materials dissolve instantly, creating a solution. Although the exact solvated species of M^{2+}, Cu^+ and Sr^{2+} are not known, conclusions could be drawn from comparisons with aqueous species. Hard cations such as Sr^{2+} probably form hydroxide coordination complexes. The borderline soft Lewis acid M^{2+} cations probably also form solvated molecular species, which is consistent with the Co concentration dependence of the formation of $[Sr_2CoO_2][Cu_2Q_2]$. These molecular complexes are probably octahedrally coordinated metal ions with OH^- ligands, such as $M(OH)_6^{4-}$. However, for the soft chalcophilic Cu^+, the complexes are more likely to be CuS_4^{7-} tetrahedra, or dimer or trimer complexes. Therefore, when these species combine to form extended compounds, they preserve their local coordination geometry. As a result, the octahedral M^{2+} complexes condense into the positively charged $[Sr_2MnO_2]^{2+}$ oxide layer and the Cu complexes into negatively charged tetrahedral chalcogenide layers.

Because the reaction is initially zero order, the concentrations of the starting materials are not the step-limiting factor. Considering that zero-order reactions are commonly seen in heterogeneous processes, fast precipitation results in a large number of nanocrystal nuclei, and the reactant concentrations decrease below the level capable of dominating the reaction. Hence, the growth at the diffusion front interface between the nanocrystals and the solution becomes the limiting factor (Fig. 4a, left and middle). As the reaction progresses to a certain level of completion, the concentration of reactants falls further and the growth becomes limited to how fast these reactants can diffuse from the opposite ends of the reaction vessel. Compared with conventional aqueous solutions, molten hydroxides are more viscous, and the diffusion rate could be one to two orders of magnitude lower than in aqueous solutions. Thus, we observe the diffusion-limited step when the reaction rate becomes low. Although the reaction could near completion in a matter of hours, the final equilibrium could take much longer to reach.

We found the sizes of the recovered crystals to be independent of cooling rate, but longer reaction times favoured bigger crystals. As the reactions can complete in 5–6 h, we attribute this growth effect over time to Ostwald ripening[45,46]. As smaller nanoparticles dissolve faster than bigger ones, the condensation of redissolved material favours bigger crystals. This is evidenced by the increasing graininess over time in the two-dimensional in situ diffraction images before integration (evolving from diffraction rings to diffraction spots). However, because of the low diffusion rate and the large number of nuclei formed during the initial precipitation, a much longer time is required to reach the final critical volume, giving a wide range of crystal size distributions.

This revealing insight into the growth mechanism of oxychalcogenides in molten bases enables us to design a diffusion-driven crystal growth route to afford much larger crystals. As the Ostwald ripening process cannot reach completion with a higher number of nuclei, decreasing the number of nuclei will certainly result in larger crystals. Hence, by suppressing the zero-order growth stage, larger crystals can be favoured by the diffusion-driven step. As shown in Fig. 4b, this is achieved by spatially separating the critical starting materials. This process is expected to be universal and highly effective, especially when multiple components are involved, and thus is of particular value for the synthesis of heterolayer structures.

Conclusions

Molten hydroxides are effective media for the controlled synthesis and crystal growth of a wide range of heterolayered oxychalcogenides. We have successfully grown crystals of these compounds using over 30 different combinations, including 15 heterolayered oxychalcogenides not previously reported. Using a wide selection of alkali hydroxides and in combination with the corresponding halides, we can control the basicity and solubility to achieve the optimal conditions for crystallizing a specific compound. Moreover, we can tune the equilibrium of the molecular species in molten bases by changing these parameters. This allows stacking of exotic layers such as $Li_6[CoSeO_2]$ to form $Li_6[CoSeO_2][Cu_2Se_2]$. By controlling the basicity, the higher oxidation states of transition metals can be stabilized in the oxide layer, and by varying the reaction temperature, the layer thickness of the copper sulfide layer can be controlled. In addition, this diffusion-driven method enables crystals one to two orders of magnitude larger than those obtained using the mixing method, and they can be further improved with longer reaction vessels and time. We have therefore advanced our understanding of the key reaction pathways that stabilize heterolayered oxychalcogenides.

Methods

To form oxychalcogenides, an alkali earth metal source (AEO or $AE(OH)_2$), a transition metal source (MCO_3, MO or MCl_2), Cu_2O (or Ag_2O) and elemental chalcogen (Q) were mixed with a flux of LiOH–LiCl or NaOH–NaI. The as-purchased NaOH that we used contained about 10–15% water by weight, and when heated, we observed this water leaving the reaction and condensing at the end of the quartz tube, especially above 200 °C. We performed our reactions in an open system and under nitrogen flow. This helped to protect the reaction from oxygen and to drive off the water from the reaction. The basicity of the LiOH–LiCl flux was controlled by the LiOH/LiCl ratio, and the compositional ratio of LiOH is defined as mol LiOH/(mol LiOH + mol LiCl). This ratio was varied between 0.5 and 1, and 0.65 gave a eutectic melt at 285 °C. For the NaOH–NaI flux with M = Mn and Cu, LiOH (LiOH/(NaOH + NaI) = 0.1–0.2) was used to substitute the Ag site for Li, which afforded larger and better crystals than the reactions without any LiOH, whereas the products showed no difference in composition with or without LiOH for M = Fe, Co, Ni and Zn as Li substitution at the Ag site was not observed for a LiOH/(NaOH + NaI) ratio up to 0.2. The reactants were typically used in a stoichiometric ratio, and the reactant to flux ratio was typically around 1:10. The ratios between the precursors were found not to affect the final product of a reaction. The reaction mixture was loaded in a rectangular glassy-carbon boat that was then placed inside a fused silica tube with each end connected to a metal valve to allow nitrogen gas to flow through. The fused silica tube was placed inside a tube furnace heated to 500–600 °C for the LiOH–LiCl fluxes and 450–500 °C for the NaOH–NaI fluxes at a heating rate of $5\,°C\,min^{-1}$. The temperature was held for 5–24 h and then the furnace was cooled naturally to room temperature by turning off the power (3–5 h for cooling). The cooling rate did not affect the final products or crystal size. The products were washed with water in an ultrasound bath to remove the flux and subsequently dried in air. The disproportion of Q led to side products such as A_2QO_x ($x = 3$ or 4), which could be fully dissolved and removed by washing with water. The yields for M = Mn, Co and Ni with Cu oxychalcogenides ranged between 80 and 90% in LiOH–LiCl, whereas the yield for M = Cu was much lower, between 30 and 50%. All reactions in NaOH/NaI gave yields of about 80%.

Data availability

The data that support the plots within this paper and other findings of this study are available in the Supplementary Information. Crystallographic data for the structures reported in this article have been deposited at the Cambridge Crystallographic Data Centre, with deposition numbers 2109506–2109520, corresponding to the compounds shown in the Supplementary Tables: **1** ($Sr_2Mn_{0.6}Cu_{1.6}Li_{0.4}S_2$, CCDC 2109509), **2** ($Sr_2Mn_{0.5}O_2Cu_{1.31}Li_{0.69}Se_2$, CCDC 2109506), **3** ($Sr_2CoO_2Cu_{1.81}S_2$, CCDC 2109519), **4** ($Sr_2CoO_2Cu_2Se_2$, CCDC 2109507), **5** ($Sr_2NiO_2Cu_2Se_2$, CCDC 2109510), **6** ($Ba_2Co_{0.54}Cu_2O_2Se_2$, CCDC 2109508), **7** ($Sr_2Mn_{0.56}O_2Ag_{1.84}Li_{0.16}Se_2$, CCDC 2109514), **8** ($Ba_3Ag_2Fe_{1.82}O_{3.73}Se_2$, CCDC 2109513), **9** ($Ba_2Co_{0.68}O_2Ag_2Se_2$, CCDC 2109515), **10** ($Ba_2Cu_{0.79}O_{1.33}Ag_{1.24}Li_{0.76}Se_2$, CCDC 2109511), **11** ($Ba_2Zn_{0.66}O_{1.42}Ag_2Se_2$, CCDC 2109512), **12** ($CoCu_2Li_{5.51}O_2Se_3$, CCDC 2109517), **13** ($SrMn_{0.5}OCu_{3.63}S_{2.5}$, CCDC 2109518), **14** ($Sr_2Ni_{0.7}O_2Cu_2Se_2$, CCDC 2109516) and **15** ($Sr_2Cu_{0.68}O_2Cu_2Se_2$, CCDC 2109520). Copies of the data can be obtained free of charge via https://www.ccdc.cam.ac.uk/structures/. Source data are provided with this paper.

Received: 8 January 2022; Accepted: 27 June 2022;
Published online: 15 August 2022

References

1. Kageyama, H. et al. Expanding frontiers in materials chemistry and physics with multiple anions. *Nat. Commun.* **9**, 772 (2018).
2. Ueda, K., Hirose, S., Kawazoe, H. & Hosono, H. Electrical and optical properties of layered oxysulfides with CuS layers: Sr−Cu−M−O−S system (M = Zn, Ga, In). *Chem. Mater.* **13**, 1880–1883 (2001).
3. Hiramatsu, H. et al. Crystal structures, optoelectronic properties, and electronic structures of layered oxychalcogenides MCuOCh (M = Bi, La; Ch = S, Se, Te): effects of electronic configurations of M^{3+} ions. *Chem. Mater.* **20**, 326–334 (2008).
4. Sheng, Z. Z. & Hermann, A. M. Bulk superconductivity at 120 K in the Tl–Ca/Ba–Cu–O system. *Nature* **332**, 138–139 (1988).
5. Kamihara, Y., Watanabe, T., Hirano, M. & Hosono, H. Iron-based layered superconductor $La[O_{1-x}F_x]FeAs$ ($x = 0.05–0.12$) with $T_c = 26$ K. *J. Am. Chem. Soc.* **130**, 3296–3297 (2008).
6. Wu, G. et al. Superconductivity at 56 K in samarium-doped SrFeAsF. *J. Phys. Condens. Matter* **21**, 142203 (2009).
7. Hsu, F.-C. et al. Superconductivity in the PbO-type structure α-FeSe. *Proc. Natl Acad. Sci. USA* **105**, 14262–14264 (2008).
8. Lu, X. F. et al. Superconductivity in $LiFeO_2Fe_2Se_2$ with anti-PbO-type spacer layers. *Phys. Rev. B* **89**, 020507 (2014).
9. Sun, H. et al. Soft chemical control of superconductivity in lithium iron selenide hydroxides $Li_{1-x}Fe_x(OH)Fe_{1-y}Se$. *Inorg. Chem.* **54**, 1958–1964 (2015).
10. Lu, X. F. et al. Coexistence of superconductivity and antiferromagnetism in $(Li_{0.8}Fe_{0.2})OHFeSe$. *Nat. Mater.* **14**, 325–329 (2015).
11. Pachmayr, U. et al. Coexistence of 3d-ferromagnetism and superconductivity in $[(Li_{1-x}Fe_x)OH](Fe_{1-y}Li_y)Se$. *Angew. Chem. Int. Ed.* **54**, 293–297 (2015).
12. Hamann, D. M. et al. Structural changes as a function of thickness in $[(SnSe)_{1+\delta}]_mTiSe_2$ heterostructures. *ACS Nano* **12**, 1285–1295 (2018).
13. Cordova, D. L. M. et al. Designed synthesis and structure–property relationships of kinetically stable $[(PbSe)_{1+\delta}]_m(VSe_2)1$ ($m = 1, 2, 3, 4$) heterostructures. *Chem. Mater.* **31**, 8473–8483 (2019).
14. Mesoza Cordova, D. L., Kam, T. M., Gannon, R. N., Lu, P. & Johnson, D. C. Controlling the self-assembly of new metastable tin vanadium selenides using composition and nanoarchitecture of precursors. *J. Am. Chem. Soc.* **142**, 13145–13154 (2020).
15. Mugavero, S. J. III, Gemmill, W. R., Roof, I. P. & zur Loye, H.-C. Materials discovery by crystal growth: lanthanide metal containing oxides of the platinum group metals (Ru, Os, Ir, Rh, Pd, Pt) from molten alkali metal hydroxides. *J. Solid State Chem.* **182**, 1950–1963 (2009).
16. Bugaris, D. E. & zur Loye, H. C. Materials discovery by flux crystal growth: quaternary and higher order oxides. *Angew. Chem. Int. Ed.* **51**, 3780–3811 (2012).
17. Bugaris, D. E., Smith, M. D. & zur Loye, H.-C. Hydroflux crystal growth of platinum group metal hydroxides: $Sr_6NaPd_2(OH)_{17}$, $Li_2Pt(OH)_6$, $Na_2Pt(OH)_6$, $Sr_2Pt(OH)_8$, and $Ba_2Pt(OH)_8$. *Inorg. Chem.* **52**, 3836–3844 (2013).
18. Chance, W. M., Bugaris, D. E., Sefat, A. S. & zur Loye, H.-C. Crystal growth of new hexahydroxometallates using a hydroflux. *Inorg. Chem.* **52**, 11723–11733 (2013).
19. Albrecht, R., Graßme, F., Doert, T. & Ruck, M. Hydroflux syntheses and crystal structures of hydrogarnets $Ba_3[RE(OH)_6]_2$ (RE = Sc, Y, Ho–Lu). *Z. Naturforsch. B* **1**, 951–957 (2020).
20. Lux, H., Kuhn, R. & Niedermaier, T. Reaktionen und Gleichgewichte in Alkalihydroxydschmelzen. III. Peroxydgleichgewichte. *Z. Anorg. Allg. Chem.* **298**, 285–301 (1959).
21. Flood, H. & Förland, T. The acidic and basic properties of oxides. *Acta Chem. Scand.* **1**, 592–606 (1947).
22. Elwell, D. & Schell, H. *Crystal Growth from High Temperature Solutions* (Academic Press, 1975).
23. Chiotti, P. & Markuszewski, R. Binary systems sodium sulfide-sodium hydroxide and sodium carbonate-sodium hydroxide. *J. Chem. Eng. Data* **30**, 197–201 (1985).
24. Seefuth, R. N. & Sharma, R. A. Solubility of Li_2S in LiCl-KCl melts. *J. Electrochem. Soc.* **135**, 796 (1988).
25. Rickard, D. & Luther, G. W. Chemistry of iron sulfides. *Chem. Rev.* **107**, 514–562 (2007).
26. Byrappa, K. & Yoshimura, M. *Handbook of Hydrothermal Technology* (William Andrew, 2012).
27. Albrecht, R. & Ruck, M. Chalcogenides by reduction of their dioxides in ultra-alkaline media. *Angew. Chem. Int. Ed.* **60**, 22570–22577 (2021).
28. Zhu, W. J. & Hor, P. H. Unusual layered transition-metal oxysulfides: $Sr_2Cu_2MO_2S_2$ (M = Mn, Zn). *J. Solid State Chem* **130**, 319–321 (1997).
29. Gál, Z. A. et al. Structural chemistry and metamagnetism of an homologous series of layered manganese oxysulfides. *J. Am. Chem. Soc.* **128**, 8530–8540 (2006).
30. Adamson, P. et al. Competing magnetic structures and the evolution of copper ion/vacancy ordering with composition in the manganite oxide chalcogenides $Sr_2MnO_2Cu_{1.5}(S_{1-x}Se_x)_2$. *Chem. Mater.* **24**, 2802–2816 (2012).
31. Jin, S. et al. $Sr_2Mn_3Sb_2O_2$ type oxyselenides: structures, magnetism, and electronic properties of $Sr_2AO_2M_2Se_2$ (A = Co, Mn; M = Cu, Ag). *Inorg. Chem.* **51**, 10185–10192 (2012).
32. Clarke, S. J. et al. Structures, physical properties, and chemistry of layered oxychalcogenides and oxypnictides. *Inorg. Chem.* **47**, 8473–8486 (2008).
33. Otzschi, K., Ogino, H., Shimoyama, J.-I. & Kishio, K. New candidates for superconductors; a series of layered oxysulfides $(Cu_2S_2)(Sr_{n+1}MnO_{3n-1})$. *J. Low Temp. Phys.* **117**, 729–733 (1999).
34. Matsumoto, Y. et al. High-pressure synthesis of $A_2NiO_2Ag_2Se_2$ (A = Sr, Ba) with a high-spin Ni^{2+} in square-planar coordination. *Angew. Chem. Int. Ed.* **58**, 756–759 (2019).
35. Cario, L. et al. Design and magnetic properties of new compounds containing iron 2D building blocks of the perovskite type. *Solid State Sci.* **7**, 936–944 (2005).
36. Salter, E. J. T., Blandy, J. N. & Clarke, S. J. Crystal and magnetic structures of the oxide sulfides CaCoSO and BaCoSO. *Inorg. Chem.* **55**, 1697–1701 (2016).
37. Cassidy, S. J. et al. Complex microstructure and magnetism in polymorphic CaFeSeO. *Inorg. Chem.* **55**, 10714–10726 (2016).
38. Dawson, J. A., Famprikis, T. & Johnston, K. E. Anti-perovskites for solid-state batteries: recent developments, current challenges and future prospects. *J. Mater. Chem. A* **9**, 18746–18772 (2021).
39. Rutt, O. J., Williams, G. R. & Clarke, S. J. Reversible lithium insertion and copper extrusion in layered oxysulfides. *Chem. Commun.* 2869–2871 (2006).
40. Blandy, J. N. et al. Synthesis, structure, and properties of the layered oxide chalcogenides $Sr_2CuO_2Cu_2S_2$ and $Sr_2CuO_2Cu_2Se_2$. *Inorg. Chem.* **57**, 15379–15388 (2018).

41. Weiland, A., Felder, J. B., McCandless, G. T. & Chan, J. Y. One Ce, two Ce, three Ce, four? An intermetallic homologous series to explore: $A_{n+1}B_nX_{3n+1}$. *Chem. Mater.* **32**, 1575–1580 (2020).
42. Bennema, P. Crystal growth from solution—theory and experiment. *J. Cryst. Growth* **24**–**25**, 76–83 (1974).
43. Pritula, I. & Sangwal, K. in *Handbook of Crystal Growth* 2nd edn (ed. Rudolph, P) 1185–1227 (Elsevier, 2015).
44. Hektisch, H. K., Dennis, J. & Hanoka, J. I. Crystal growth in gels. *J. Phys. Chem. Solids* **26**, 493–496 (1965).
45. Voorhees, P. W. The theory of Ostwald ripening. *J. Stat. Phys.* **38**, 231–252 (1985).
46. Baldan, A. Review progress in Ostwald ripening theories and their applications to nickel-base superalloys part I: Ostwald ripening theories. *J. Mater. Sci.* **37**, 2171–2202 (2002).
47. Smura, C. F. et al. High-spin cobalt(II) ions in square planar coordination: structures and magnetism of the oxysulfides $Sr_2CoO_2Cu_2S_2$ and $Ba_2CoO_2Cu_2S_2$ and their solid solution. *J. Am. Chem. Soc.* **133**, 2691–2705 (2011).
48. Ueda, K. & Hosono, H. Crystal structure of $LaCuOS_{1-x}Se_x$ oxychalcogenides. *Thin Solid Films* **411**, 115–118 (2002).
49. Ohki, Y., Takase, K., Takahashi, Y., Takano, Y. & Sekizawa, K. Preparation and crystal structure analysis and physical properties of (LaO)CuTe. *J. Alloys Compd* **408**–**412**, 98–100 (2006).
50. Zhou, T. et al. Structures and physical properties of layered oxyselenides $Ba_2MO_2Ag_2Se_2$ (M = Co, Mn). *Inorg. Chem.* **53**, 4154–4160 (2014).
51. Herkelrath, S. J. C., Saratovsky, I., Hadermann, J. & Clarke, S. J. Fragmentation of an infinite ZnO_2 square plane into discrete $[ZnO_2]^{2-}$ linear units in the oxyselenide $Ba_2ZnO_2Ag_2Se_2$. *J. Am. Chem. Soc.* **130**, 14426–14427 (2008).

Acknowledgements

This work was supported by the US Department of Energy, Office of Science, Basic Energy Sciences, Materials Sciences and Engineering Division. Use of the Center for Nanoscale Materials, including SEM and the ACAT, an Office of Science user facility, was supported by the US Department of Energy, Office of Science, Office of Basic Energy Sciences, under contract no. DE-AC02-06CH11357. Work at the beamlines 17-BM-B, 15-ID and 20-BM-B at the Advanced Photon Source at Argonne National Laboratory was supported by the US Department of Energy, Office of Science, Office of Basic Energy Sciences under contract no. DE-AC02-06CH11357. NSF's ChemMatCARS Sector 15 is supported by the Divisions of Chemistry (CHE) and Materials Research (DMR), National Science Foundation, under grant number NSF/CHE-1834750.

Author contributions

The work was conceived by X.Z., D.Y.C. and M.G.K. with input from all authors. X.Z. carried out the synthesis, laboratory X-ray diffraction and elemental analysis. C.D.M. and X.Z. analysed the single-crystal diffraction data. X.Z., A.Y. and B.W. collected and analysed the in situ diffraction data. S.G.W. and Y.-S.C. collected the synchrotron single-crystal diffraction data. J.W. performed the TEM analysis and J.W. and L.Y. analysed the EELS spectra. M.B. carried out the XAS experiments. H.-H.W. collected the Raman spectra. D.-Y.C. and M.G.K. supervised the project.

Competing interests

The authors declare no competing interests.

Additional information

Supplementary information The online version contains supplementary material available at https://doi.org/10.1038/s44160-022-00130-4.

Correspondence and requests for materials should be addressed to Mercouri G. Kanatzidis.

Peer review information *Nature Synthesis* thanks Xiaolong Chen and the other, anonymous, reviewer(s) for their contribution to the peer review of this work. Primary Handling Editor: Peter Seavill, in collaboration with the *Nature Synthesis* team.

Reprints and permissions information is available at www.nature.com/reprints.